https://doi.org/10.1007/s41230-025-4017-1

Effect of heat treatment on microstructure and mechanical properties of a novel Al-Zn-Mg-Cu alloy

Yan-mei Yang[1], Xin-chen Tang[1], *Ye-fei Li[1], Xue-wei Fang[1], Da-wei Yi[1], Zhi-yun Zhang[1], Qiao-ling Zheng[1], Zhi-xi Wang[1], Guo-yu Zhang[1], Su Zhang[2], Hao Cheng[2], Yang He[1], Yi-bo Liu[1], Zi-han Wu[1], Ya-nan Chen[1], and Yi-min Gao[1]

1. State Key Laboratory for Mechanical Behavior of Materials, Xi'an Jiaotong University, Xi'an 710049, China

2. Xi'an Aerospace Precision Electromechanical Institute, Xi'an 710100, China

Abstract: Effects of solution and aging treatment on the microstructure and mechanical properties of a novel Al-Zn-Mg-Cu alloy by microalloying rare elements Sc and Er were studied. The results show that solution time has a visible influence on the microstructure and mechanical properties of the alloy. Specifically, as the solution time increases, the area fraction of the residual phase in the alloy decreases, and the shape of the grain becomes more spheroidal and coarser, leading to a decrease in hardness. This is attributed to the dissolution of strengthening phases during the solution treatment, which weakens the solid solution strengthening effect. The single-stage aging treatment shows an initial increase in strength and hardness of the alloy, followed by a decrease as the aging time is extended, until a steady state is achieved. The optimal single-aging conditions are found to be at 120 °C for 24 h, where the alloy exhibits an excellent combination of high strength and good ductility, with an ultimate tensile strength (UTS) of 523 MPa, yield strength (YS) of 482 MPa, and elongation (El) of 1.75%, respectively. Compared to single-stage aging, double-stage aging (120 °C for 24 h and then 150 °C for 52 h) significantly increases the elongation of the alloy (4.17%), but the UTS reduces to 465.29 MPa, and YS reduces to 410.64 MPa. Transmission electron microscopy (TEM) observations disclose that the grain size, the distribution spacing of precipitates along the grain boundary, and the width of the precipitation-free zone (PFZ) all undergo augmentation as the duration of the second stage aging process elongates.

Keywords: Al-Zn-Mg-Cu alloy; aging treatment; strength; precipitate free zone

CLC numbers: TG146.21 **Document code:** A **Article ID:** 1672-6421(2025)03-292-09

1 Introduction

High-strength, precipitation-hardened 7xxx series Al-Zn-Mg-Cu alloys, characterized by their advanced age-hardening response, are widely utilized in the fabrication of critical aircraft structural components, where they are exposed to stringent conditions. Strength, ductility, modulus, corrosion resistance, and damage tolerance (such as fatigue resistance and fracture toughness) are crucial characteristics that need to be taken into account for these applications. With suitable elemental alloying, processing and heat treatment, Al-Zn-Mg-Cu alloys could be applied more widely in the aerospace industry due to their remarkable properties [1,2].

In order to meet the high requirements of modern industry, the micro-alloying technology, as an effective method, has been widely applied to improve the comprehensive performance of many aluminum alloys, including Al-Zn-Mg-Cu alloys. Sc and Zr transition metals, as well as Er could react with liquid aluminum and form thermodynamically stable dispersed phases known as Al_3M trialuminides. These phases have a similar crystal structure and lower lattice parameter mismatch in relation to the α-Al matrix [3, 4].

The addition of Sc has a strong refining effect on the grain structure of Al-matrix and forms a super saturated solid solution during solidification. Fine, coherent precipitates with an $L1_2$ structure, specifically Al_3Sc, can form during the decomposition of an Al-Sc solid solution [5-7]. Scanium (Sc) enhances the recrystallization resistance of the alloys. It is reported

***Ye-fei Li**

Associate Professor. His research interests mainly focus on the fields of advanced wear resistant materials, the design and preparation of metal matrix composites, computational materials science, and related fields. He has led and contributed to many scientific projects, including those founded by NSFC. To date, he has authored over 100 scientific publications.

E-mail: liyefei@xjtu.edu.cn

Received: 2024-01-27; Revised: 2024-06-23; Accepted: 2024-08-27

that recrystallization of aluminum alloys containing Sc occurs at temperatures above 375 °C, which is about 100 °C higher than that of Sc free alloys [8]. Li et al. [9] investigated the effects of minor Sc on the microstructure and mechanical properties of Al-Zn-Mg-Cu-Zr based alloys. With the addition of 0.21% Sc, both the ultimate tensile strength and yield strength were improved greatly. Additionally, the as-cast crystal grains were refined and the recrystallization of the studied alloys was strongly retarded. Similar to Sc, the heaviest rare earth element erbium (Er) can partially or fully substitute for Sc in the $L1_2$ structured Al_3(Sc, Er) phase [10]. This substitution is found to enhance the strength and refine the grains by forming the Al_3Er phase. The dispersed nanosized Al_3Er phase serves as the sites for heterogeneous nucleation of the η($MgZn_2$) phase, which results in grain refinement and an improvement in mechanical properties, and at the same time reduce the cost of alloys [11]. Li et al. [12] studied the effect of Er addition on microstructure and mechanical properties of Al-20% Si alloy. It has been found that Er can significantly refine the primary Si crystals and modify eutectic Si structure, finally promote the ultimate tensile strength and elongation of the alloy. Zirconium (Zr) also could improve the strength by suppressing recrystallization and refining grains [13]. Shi et al. [14] studied the effect of Zr addition on the microstructural evolution of AA7150 aluminum alloy, which shows that Zr could inhibit the dynamic recrystallization and dislocation motion. Fortunately, combined addition of rare earth elements (Sc, Er) and transition elements (Zr) to aluminum alloys can yield remarkable enhancements in the alloy's overall performance due to the formation of thermally stable coherent $L1_2$-stuctured Al_3M ($M=Sc_xEr_{1-x}$ or Er_xZr_{1-x},etc) nanoparticles [15].

Considerable research works have shown that the combination of microalloying and heat treatment enables the alloy to achieve ideal comprehensive properties [16]. Thus, in order to further improve the mechanical properties, Al-Zn-Mg-Cu alloys are often subjected to different heat treatments, including homogenization, solution, and aging. Solution treatment is the first step required to determine the final properties of Al alloy, and its role is to redissolve the residual phases into α(Al) matrix as much as possible [17]. Wang et al. [18] investigated the effect of solution treatment on microstructural and mechanical properties of Al-9.0Zn-2.8Mg-2.5Cu-0.12Zr-0.03Sc alloy. The results showed that solution treatment could avoid the recrystallization of alloy with minor additions of Sc (<0.1%), and acquired the peak value of tensile strength. Solution treatment could also minimize second phases, promote uniform passive film thickness and uniform solute segregation, offering insights for improving corrosion resistance [19, 20]. As is known, Al-Zn-Mg-Cu alloy is an typical aging-strengthened aluminum alloy. The aging process effectively promotes the precipitation of the second phases in the supersaturated solid solution [21], which are dispersed throughout the Al matrix. This impedes the movement of grain boundaries and dislocations, ultimately enhancing the strength of the alloy. High strength can be reached by single-stage or double-stage aging treatments [2]. In most cases, double-stage aging produces finer precipitation phases and enhance mechanical strength than single-stage aging. This process can regulate the comprehensive properties of aluminum alloys by optimizing the distribution and size of the precipitates [22-25].

Extensive research has been conducted by scholars in the domain of heat treatment systems [4, 10-12, 26]. Nevertheless, the effect of both alloying process and single/dual-stage aging heat treatment on high-Zn 7xxxx alloys is somewhat insufficient. The current work focuses on a typical high-Zn aluminum alloy with low-Cu content, and trace amounts of the rare earth elements Sc and Er, as well as transition metal Zr. The objective is to develop a new choise for the utilization of aluminum alloys in aerospace production.

2 Materials and experimental methods

The experimental procedure involved the use of a vacuum induction melting furnace to produce a self-made 7xxx series aluminum alloy. The ingot was subsequently homogenized at a temperature of 465 °C for a duration of 24 h, based on the findings from differential scanning calorimetry (DSC) analysis. The distinct phase transformation temperatures of the alloy were determined through DSC tests conducted using a 250 DSC machine. These tests involved heating the sample from room temperature to 700 °C at a rate of 10 $°C·min^{-1}$ with argon gas serving as the protective shielding atmosphere. Following the homogenized process, the nominal chemical elements of the ingot were meticulously analyzed using inductively coupled plasma (ICP) spectroscopy. Table 1 presents the nominal and measured values of the alloy's chemical composition.

Figure 1 illustrates the schematic diagram of the heat treatment process for the alloys, while Table 2 details the heat treatment parameters, including the single-stage aging and double-stage aging following the solution treatment. Hardness measurements were performed using a RTD700 Rockwell hardness tester, applying a load of 588.24 N for a duration of 10 s. Compliance with the GB/T228.1-2010 standard, the tensile properties reported were the mean values obtained from three samples per condition, tested on an Instron 5982 machine. The microstructure was examined using polarized light microscopy, and the phase constitution of the alloy at various states were observed and analyzed using a scanning electron microscopy (SEM) equipped with an energy dispersive X-ray spectroscopy (EDS). To

Table 1: Chemical composition of the experimental alloy (wt.%)

Composition	Si	Fe	Cu	Mg	Mn	Zr	Zn	Ti	Sc	Er	Al
Nominal value	<0.05	<0.05	1.6	2.2	0.10	0.15	6.10	0.10	0.15	0.15	Bal.
Measured value	0.02	0.05	1.51	2.13	0.10	0.16	6.16	0.10	0.16	0.18	Bal.

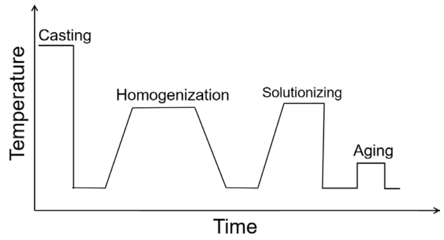

Fig. 1: Schematic diagram of heat treatment process for the investigated aluminum alloy

analyze the precipitates, a transmission electron microscope (TEM-JEM-3010) was employed, and the TEM samples were prepared via twin-jet polishing with an electrolyte solution (30vol.% of HNO_3 and 70vol.% of CH_3OH) at a voltage of 15 V within a temperature range of 25 °C to 30 °C. The alloy trace composition was analyzed by wavelength dispersive spectroscopy (WDS) using an electron probe micro analyzer (EPMA, JXA-iHP200F).

Table 2: Different heat treatment processes of the aluminum alloy

Homogenization	Solutionizing	Aging
465 °C /24 h	470 °C/(30, 60, 90, 120 min)	120 °C/(3, 6, 12, 24, 48, 72, 96 h) 120 °C/8 h+(130, 140, 150 °C)/(16, 28, 52, 76, 100 h)

3 Results

3.1 Microstructure

Figure 2 shows the polarized light metallographic structure and SEM images of the alloy at as-cast and homogeneous states. The as-cast structure exhibits a classic dendritic structure [Fig. 2(a)], with an average grain size of approximately 25 μm. Segregation is evident within the ingot [Fig. 2(b)], and the presence of numerous non-equilibrium precipitated phases is observed at the grain boundaries, as well as granular precipitation phases within the grains. Table 3 presents the results of the quantitative EDS analysIs of positions marked in Fig. 2(c). These analysis results indicate that the white granular precipitation phase (Position 1) is predominantly Al_3(Sc, Zr, Ti). Meanwhile, the white long rod-like precipitated phase at grain boundary (Position 2) is identified as Al_8Cu_4Er. Elemental composition analysis was conducted by means of EPMA. A representative mapping image is displayed in Fig. 2(g), which reveals that the elements Er and Cu are primarily enriched at the grain boundaries. EDS analysis further confirms that Sc, Zr, and Ti elements predominantly form bulk precipitates within the grain matrix.

Figure 2(f) presents the results of DSC of the alloy, which presents a distinct endothermic peak at 476.5 °C. Typically, the homogenization temperature should be set approximately 10 °C below this peak temperature to avoid overheating. Consequently, a homogenization temperature of 465 °C is chosen for this study. The microstructure of the alloy after homogenization treatment at 465 °C for 24 h is shown in Figs. 2(d–e). Following the homogenization process, the majority of the second phases dissolves into the α-Al matrix. The grains have undergone significant merging and growth, with the average grain size increasing by approximately 10 μm. The continuous second phases that are originally distributed along the grain boundaries in the as-cast state become discontinuous after homogenization, as depicted in Fig. 2(e). This transformation indicates a more uniform distribution of elements and a reduction in micro segregation, which is beneficial for improving the mechanical properties and workability of the novel alloy.

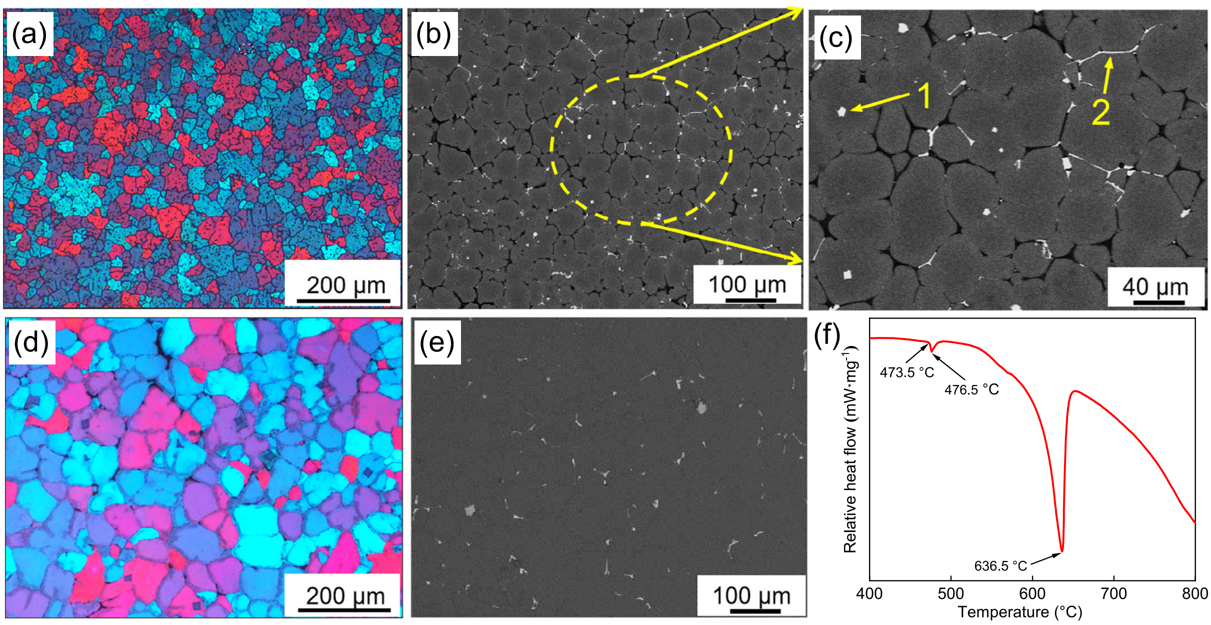

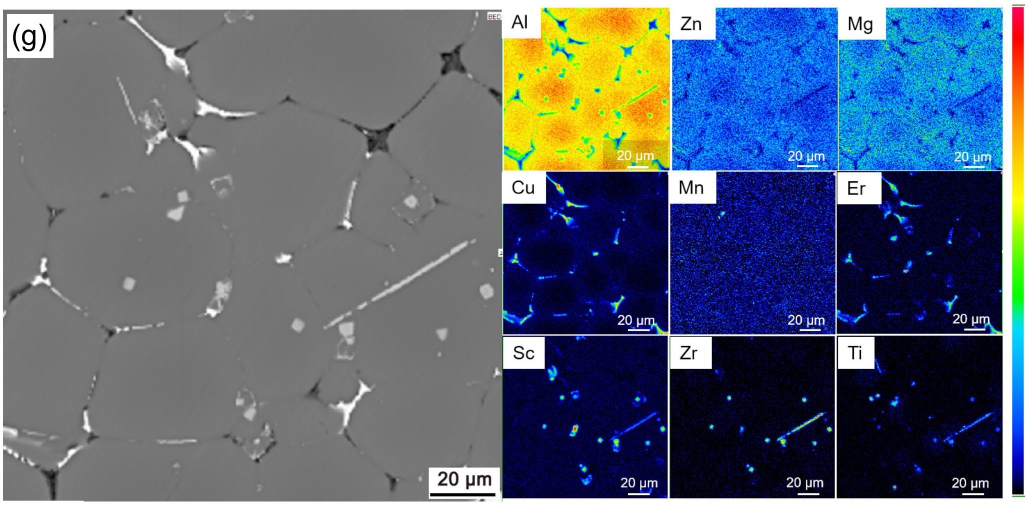

Fig. 2: Polarized light microstructure (a), SEM in low magnification (b) and high magnification (c) of the as-cast alloy; polarized light microstructure (d) and SEM (e) of the alloy after homogenization at 465 °C for 24 h; DSC curve (f) and EPMA mapping image (g) of as-cast alloy

Table 3: EDS elemental analyses of positions marked in Fig. 2(c) (at.%)

Position	Al	Mg	Zn	Cu	Sc	Zr	Er	Ti	Mn
1	81.42	1.01	2.89	0.33	3.73	7.72	0.07	2.75	0.06
2	10.54	1.36	3.57	80.67	0.49	0.06	3.14	0.03	0.11

3.2 Effect of solution treatment

The primary objectives of solution treatment in aluminum alloys are to maximize the dissolution of second-phase particles into the supersaturated solid solution and to enable the subsequent precipitation of nanoscale phases during the artificial aging process [21, 27, 28]. Figures 3(a–d) illustrate the metallographic structure and grain size distribution of the alloy at various solution treatment times. The microstructure of the solution treated sample remains largely unchanged with the prolongation of the holding time. A modest increase in average grain size is observed, with the grain size distribution maintaining a monotonic trend. The average grain sizes for the samples are 53.09, 54.46, 55.78, and 57.33 μm, respectively, indicating a gradual growth in grain size as the solution time extends.

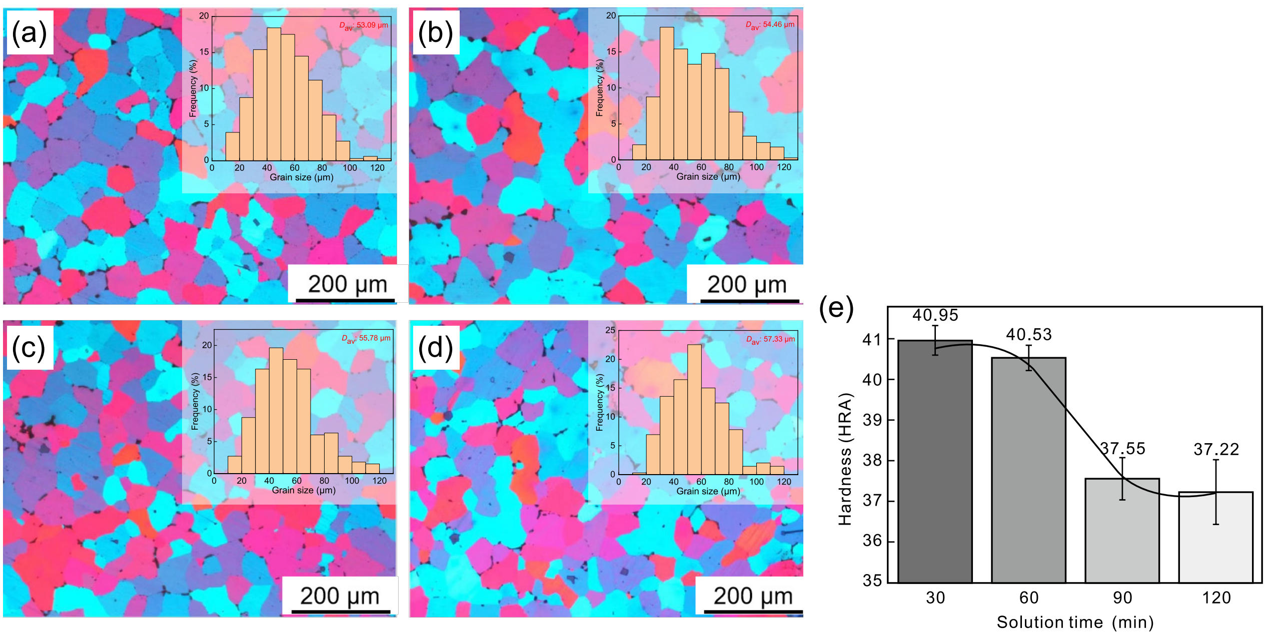

Fig. 3: Metallographic structure diagram, grain size distribution, and hardness of the alloy solution treated at 470 °C for different times: (a) 30 min; (b) 60 min; (c) 90 min; (d) 120 min; and (e) hardness

Figure 3(e) reveals the mechanical properties of the alloy after solution treatment at 470 °C for different durations. The solution time markedly influences the hardness of the alloy, with hardness decreasing as the holding time increases. The increase in solution time on the novel Al-Zn-Mg-Cu alloy enhances the dissolution of second phases. This is evident from the interdendritic phase volume fractions of the alloy solution treated at 470 °C for durations of 30, 60, 90, and 120 min, which are 0.34%, 0.16%, 0.14%, and 0.09%, respectively (Fig. 4). To some extent, the greater the decrease in hardness, the more effective the solution treatment. The long duration of the solution treatment makes the solute atoms fully and uniformly distributed in the alloy. However, with the further extension of the solution time, coarsening second phase precipitates and grains gradually grow up, which may weaken the second phase strengthening effect and soften the alloy, ultimately reducing the hardness of the alloy [Fig. 3(e)]. Based on these findings, the optimal solution treatment process for the alloy was determined to be at 470 °C for 90 min. Subsequent studies have been conducted using this established solution treatment protocol.

3.3 Effect of single-stage aging on properties of the alloy

Figure 5 depicts the changes in hardness and tensile properties of the alloy at an aging temperature of 120 °C for various aging times: 3 h, 6 h, 12 h, 24 h, 48 h, 72 h, and 96 h, respectively. As observed in Fig. 5(a), the studied alloy exhibits obvious age hardening behavior. At the start of the aging process (0 h), the alloy has an initial Rockwell hardness of 37.69 HRA. As the aging time increases, the hardness of the alloy shows a significant initial increase during the early stage of aging (under-aging). At 3 h of aging, the hardness jumps to 56.03 HRA, reaching its peak value of 59.09 HRA after 24 h (peak-aging). Subsequently, the hardness slightly decreases and then remains relatively stable over an extended period (over-aging), indicating that the alloy has entered a state of equilibrium where the rate of precipitation and coarsening of the strengthening phases is balanced.

Figure 5(b) shows the tensile properties of the alloy at various aging times. It is evident that both the ultimate tensile strength (UTS) and yield strength (YS) of the alloy initially

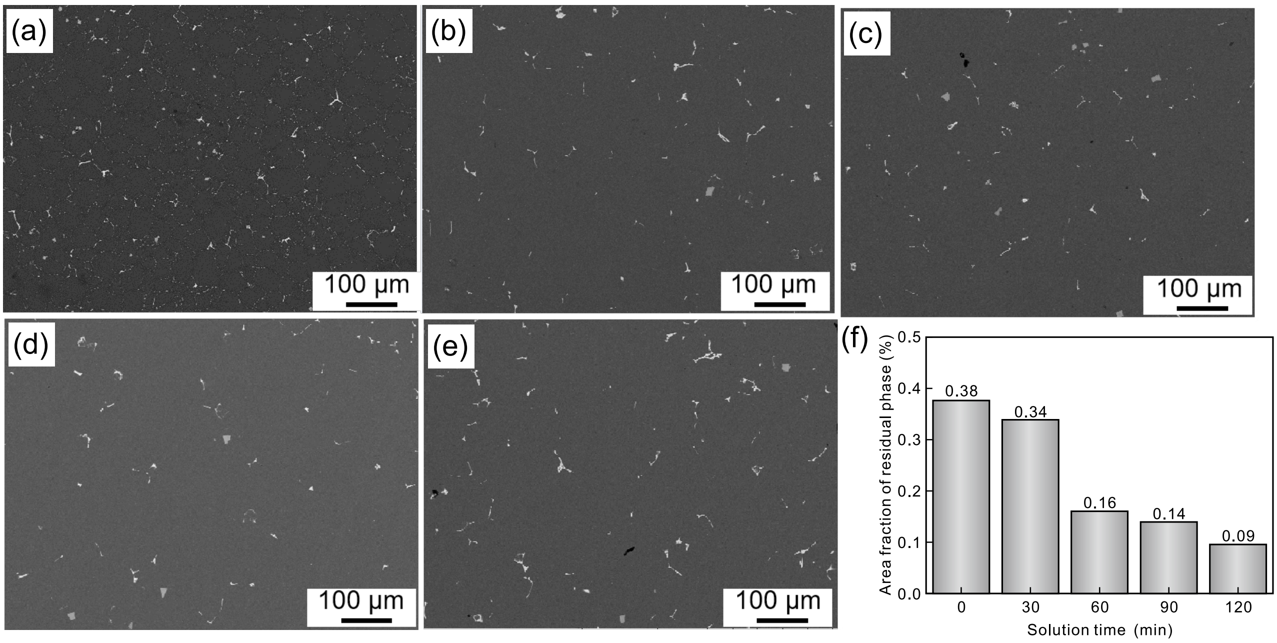

Fig. 4: SEM images of the studied alloys solutioned at 470 °C for different times: (a) 0 min; (b) 30 min; (c) 60 min; (d) 90 min; (e)120 min; and (f) area fraction of residual phase of different solution times

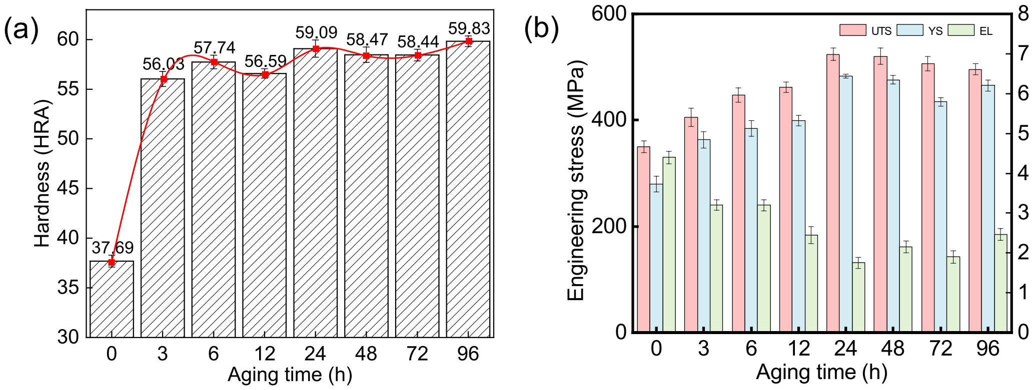

Fig. 5: Effect of single stage aging on hardness (a) and tensile properties (b) of the alloy

increase and then decrease as the aging time is prolonged. In contrast, the elongation (EL) of the alloy exhibits the opposite trend. Specifically, when aged at 120 °C for 3 h, 6 h, 12 h, and 24 h, both the UTS and YS of the alloy show an upward trend with increasing the aging time. The alloy achieves its maximum tensile properties at 120 °C for 24 h, with a UTS of 523 MPa, a YS of 482 MPa, and an EL of 1.75%. However, as the aging time extends from 24 h to 48 h, the alloy transitions from the peak-aged to the over-aged state, and the UTS and YS begin to decline slightly. After an aging treatment at 120 °C for 96 h, the peak values of UTS and YS decrease by 28 MPa and 17 MPa, respectively, indicating that the alloy has undergone excessive aging, leading to a gradual loss of strength. With the extension of aging time, both UTS and YS increase, while the EL decreases. The mechanical properties of the alloy in the peak-aged state (24 h) reach a good combination of UTS and YS. Consequently, the best single-stage aging regime for the alloy is aged at 120 °C for 24 h, based on the analysis of hardness and tensile properties.

Generally, the precipitation sequence of Al-Zn-Mg-Cu alloy in the aging process is as follows: supersaturated solid solution (SSS)→GP zones→ metastable η' ($MgZn_2$)→stable η ($MgZn_2$) [16, 29]. Among them, the GP zone and the η' phase are the main reinforcement phases. For 7xxx series Al alloy, different aging treatments will cause different changes in the metallographic structure and mechanical properties of the alloy. The properties of the alloy are directly affected by the structure and morphology of the precipitated phases on the boundary. Figure 6 shows the TEM microstructures of the alloys after aged at 120 °C for different times. After aging treatment for 6 h [Fig. 6(a)], it is evident that the GP zones form with a high density and are distributed within α(Al) matrix. Additionally, the precipitates η'($MgZn_2$) along grain boundaries are continuous and their sizes are small [Fig. 6(d)]. Meanwhile, precipitation free zone (PFZ) is formed with the size of around 55 nm. After aging treatment at 120 °C for 24 h, more precipitates transform from metastable η' precipitates to stable η precipitates with the increasing aging time. The η precipitates are distinctly coarsening and completely discontinuous along grain boundary [Fig. 6(e)]. When the aging time reaches 72 h, both the distribution spacing and grain size of the precipitates along the grain boundary undergo further enlargement. The PFZ, with the size of around 569 nm in width, can be easily observed along grain boundaries [Fig. 6(f)]. The relatively small size of $MgZn_2$ phase, GP zones, and PFZ present in the peak-aged alloy serve to robustly obstruct the migration of dislocations, thereby markedly enhancing the tensile strength of the alloy. The observed decrease in ductility for the alloy that has been aged at 120 °C can be ascribed to the growth of the $MgZn_2$ phase. With the increasing aging time, the distribution density of GP zones decreases, larger size of $MgZn_2$ and PFZ forms, which lead to the decrease in mechanical properties of the alloy.

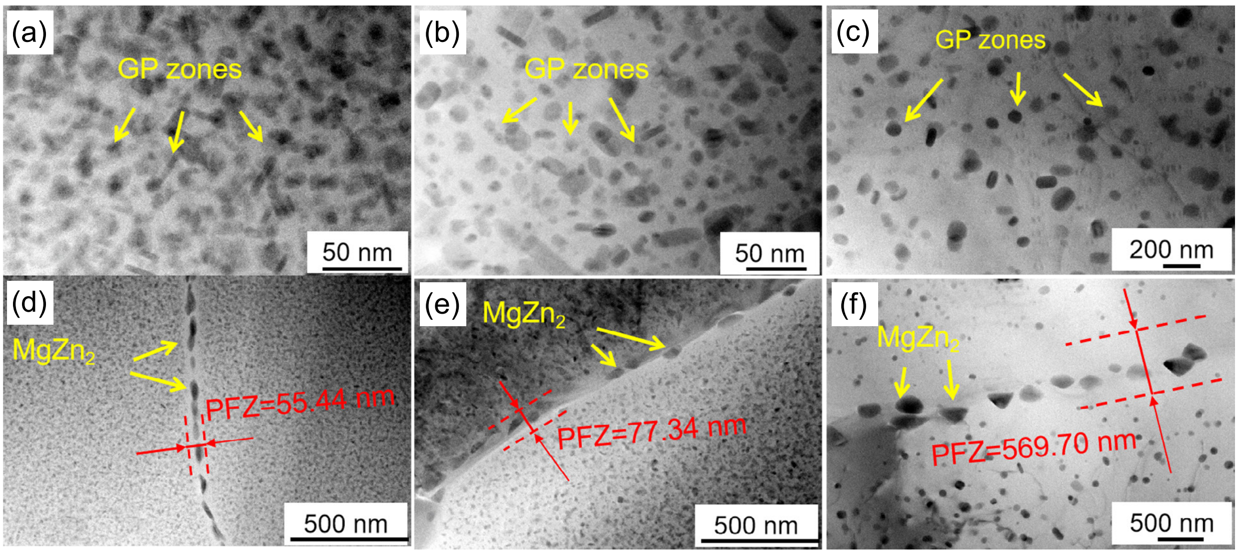

Fig. 6: TEM images of studied alloy after aged at 120 °C for various durations: (a, d) 6 h; (b, e) 24 h; (c, f) 72 h

3.4 Effect of double-stage aging on properties of alloy

Figure 7 depicts the hardness of the specimens during different double-stage aging processes. The trend in hardness variation is largely consistent across various secondary aging temperatures. The alloy quickly attains its peak hardness after 16 h of secondary aging and then exhibits a gradual downward trend as the aging time increases. It is observed that higher aging temperatures expedite the attainment of peak hardness of the alloy.

Table 4 reveals the tensile properties of the alloy after various secondary aging treatments. For a given secondary aging temperature, both the UTS and YS of the alloy initially increase and then decrease as the aging time is extended, except aging at 130 °C, while the EL fluctuates slightly, typically within the range of 2% to 4%. This behavior is consistent with the typical aging response of aluminum alloys, where the alloy reaches a peak strength and then gradually overages, leading to a decline in mechanical properties. As the secondary aging temperature rises and the aging time prolongs,

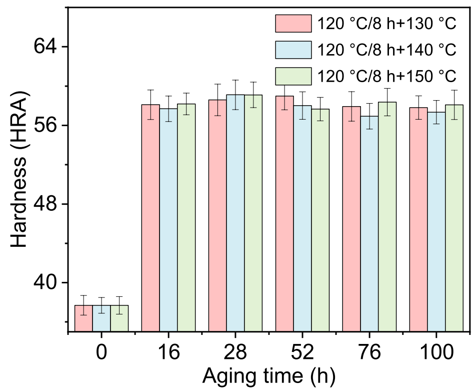

Fig. 7: Effect of double-stage aging on hardness of the alloy

the decreases in tensile strength and yield strength become more pronounced. For instance, at a secondary aging temperature of 130 °C, the UTS and YS of the alloy decrease from 519.19 MPa and 450.61 MPa to 452.88 MPa and 436.13 MPa, respectively, representing reductions of 12.77% and 3.32%, when the aging time is increased from 16 h to 100 h. Similarly, at 140 °C, the losses in UTS and YS are 4.91% and 19.66%, and at 150 °C, they are reduced by 15.62% and 23.90%, respectively. The data in Table 4 also indicate that the optimal balance of strength and plasticity is achieved when the alloy is aged for 52 h across different secondary aging temperatures. This suggests that there is an optimal aging time window for each temperature that maximizes the alloy's mechanical properties, beyond which over aging begins to occur, leading to a gradual deterioration in performance. The decrease in mechanical properties of the alloy during aging is indeed closely related to the coarsening of precipitated phases and the significant widening of PFZ.

Table 4: Effect of double-stage aging on mechanical properties of the Al-Zn-Mg-Cu alloy

Temperature	Second aging	UTS (MPa)	YS (MPa)	EL (%)
130 °C	16 h	519.19±5	450.61±3	3.73±0.3
	28 h	482.98±4	450.25±4	1.83±0.5
	52 h	514.77±5	454.45±5	2.34±0.4
	76 h	506.96±6	460.27±4	1.73±0.5
	100 h	452.88±5	436.13±6	1.97±0.2
140 °C	16 h	377.64±4	360.33±5	2.07±0.2
	28 h	377.68±3	337.18±5	2.37±0.4
	52 h	381.65±5	321.31±4	2.14±0.3
	76 h	374.72±4	342.13±4	1.47±0.3
	100 h	359.09±6	289.47±2	1.63±0.2
150 °C	16 h	342.03±3	342.32±4	3.77±0.3
	28 h	440.94±4	486.01±2	3.43±0.2
	52 h	465.29±3	410.64±3	4.17±0.4
	76 h	312.13±2	274.17±4	3.12±0.3
	100 h	288.67±6	260.52±3	3.47±0.2

The bright-field TEM images in Fig. 8 illustrate the matrix strengthening phases in the investigated alloy at various secondary aging temperatures for an aging time of 52 h. Three conditions reveal a high density of finely dispersed η' phases. As depicted in Figs. 8(a–c), the η' phases are comparatively well-distributed. However, as depicted in Figs. 8(a_1–c_1), it is evident that with the elevation of the secondary aging temperature, the width of the PFZ at the grain boundaries, as well as the coarsening of the precipitation phase at grain boundaries, incrementally widens from around 74 nm to 170 nm. This phenomenon is accompanied by a gradual reduction in the tensile strength of the alloy.

The optimized heat treatment process illustrated in Fig. 9 demonstrates remarkable advancements compared to Refs. [30–34]. This optimized process results in enhanced strength for the alloy. Additionally, a significantly greater strength can be attained through single-stage aging, while a notably higher elongation can be achieved through double-stage aging. Zhang et al. [30] investigated an Al-Zn-Mg-Cu alloy with the addition of Si-Zr-Er, the optimum single-stage aging heat treatment regime was finally obtained as 150 °C×4 h, and its mechanical properties are slightly lower than those of the present experimental alloy. Another study involved the incorporation of Sc, Cr, and Zr as microalloying elements into a high-strength, high-ductility Al-Zn-Mg-Cu alloy, followed by

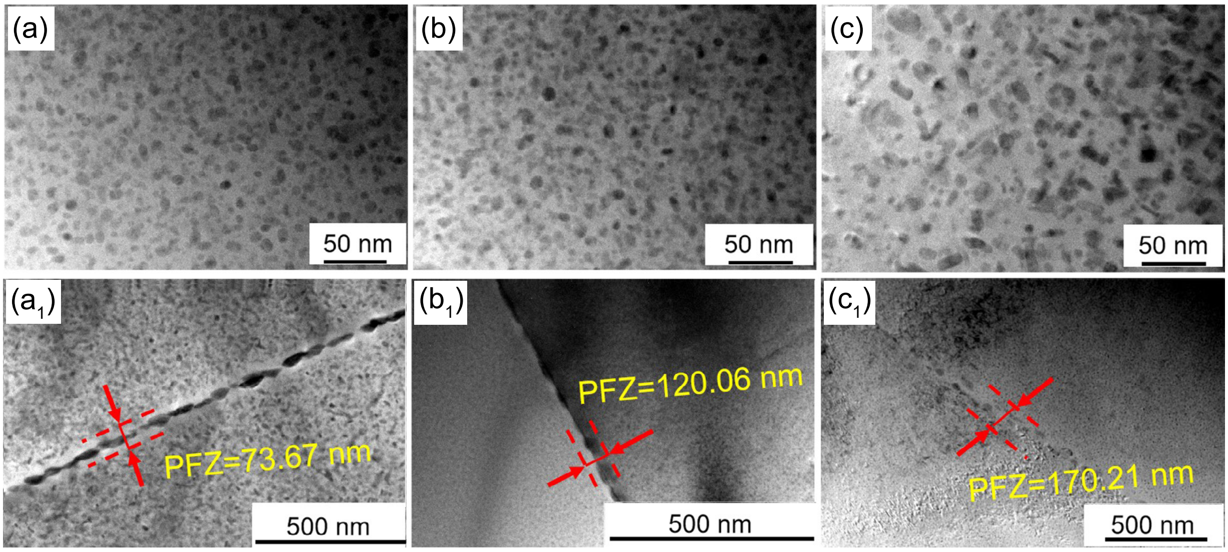

Fig. 8: TEM images of studied alloy after aged for 52 h at different secondary aging temperatures: (a–a_1) 130 °C; (b–b_1) 140 °C; (c–c_1) 150 °C

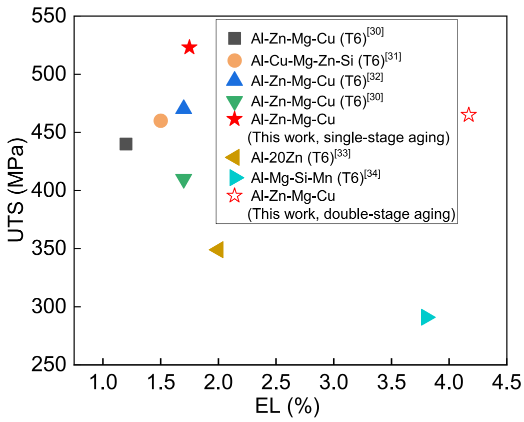

Fig. 9: Comparison of UTS versus EL for the studied alloy with the reported Al-Zn-Mg alloys [30-34]

a comprehensive T6 heat treatment process [34], with the aim of achieving high elongation. The strength of the alloy subjected to the full T6 process was notably lower than that of the current experimental alloy. Consequently, by employing an optimal heat treatment process, alloys can be tailored to exhibit exceptional performance, with the present experimental alloy surpassing other aluminum alloys in terms of overall performance.

4 Conclusions

This study examined the mechanical properties and microstructural evolution of the 7150 alloy, which has been further alloyed with Sc and Er, and subjected to various heat treatment processes. Effect of single-aging and double-aging processes on the alloy's mechanical characteristics and microstructural alterations were studied, utilizing SEM, TEM, and EPMA techniques. Through meticulous investigation, the profound impact of Sc and Er elements on the hardening behavior of the alloy has been examined. Based on our observations, the following conclusions can be drawn:

(1) In solid solution treatment, with the increase of solution time, the hardness of the alloy decreases. When solution at 470 °C for 90 min, good comprehensive mechanical performances can be obtained, and the hardness reaches 37.55 HRA.

(2) The strength and hardness of the alloy gradually increase with the extension of single-stage aging time, reaching a peak at 24 h. This peak is characterized by ultimate tensile strength of 523.74 MPa, yield strength of 482.67 MPa, and hardness of 59.09 HRA. However, with the extension of aging time, the mechanical properties of the alloy decrease due to the coarsening of the precipitated phases and widening of precipitation free zone at grain boundaries.

(3) The optimal double-stage aging treatment for the alloy, as determined by evaluating hardness, strength, and elongation, is as follows: an initial aging at 120 °C for 8 h, followed by a second aging at 150 °C for 52 h. This treatment yields a hardness of 57.66 HRA, an ultimate tensile strength of 465.29 MPa, a yield strength of 410.64 MPa, and an elongation of 4.17%.

Acknowledgments

This work was funded by the Qin Chuangyuan "Scientist and Engineer" Team Construction Project of Shaanxi Province (No. 2024QCY-KXJ-041), the Xi'an Science and Technology Program (Nos. 23LLRH0032, 23ZDCYJSGG0047-2022), and the State Key Laboratory for Mechanical Behavior of Materials (No. 20232508). We also thank Ms. Ya-nan Chen at Instrument Analysis Center of Xi'an Jiaotong University for their assistance with SEM analysis, the National Training Program of Innovation and Entrepreneurship for Undergraduates.

Conflict of interest

The authors declare that they have no known competing financial interests or personal relationships that could have appeared to influence the work reported in this paper.

References

[1] Dursun T, Soutis C. Recent developments in advanced aircraft aluminium alloys. Materials & Design, 2014, 56: 862–871.

[2] Rometsch P A, Zhang Y, Knight S. Heat treatment of 7xxx series aluminium alloys – Some recent developments. Transactions of Nonferrous Metals Society of China, 2014, 24(7): 2003–2017.

[3] Trudonoshyn O, Prach O, Randelzhofer P, et al. Heat treatment of the new high-strength high-ductility Al-Mg-Si-Mn alloys with Sc, Zr and Cr additions. Materialia, 2021, 15: 100981.

[4] Li B, Pan Q, Huang X, et al. Microstructures and properties of Al-Zn-Mg-Mn alloy with trace amounts of Sc and Zr. Materials Science and Engineering: A, 2014, 616: 219–228.

[5] Li Y, Liu Z, Xia Q, et al. Grain refinement of the Al-Cu-Mg-Ag alloy with Er and Sc additions. Metallurgical and Materials Transactions: A, 2007, 38(11): 2853–2858.

[6] Shi Y, Pan Q, Li M, et al. Effect of Sc and Zr additions on corrosion behaviour of Al-Zn-Mg-Cu alloys. Journal of Alloys and Compounds, 2014, 612: 42–50.

[7] Tian S, Li J, Zhang J, et al. Effect of Zr and Sc on microstructure and properties of 7136 aluminum alloy. Journal of Materials Research and Technology, 2019, 8(5): 4130–4140.

[8] Mondol S, Kumar S, Chattopadhyay K. Effect of thermo-mechanical treatment on microstructure and tensile properties of 2219ScMg alloy. Materials Science and Engineering: A, 2019, 759: 583–593.

[9] Li W, Pan Q, Zou L, et al. Effects of minor Sc on the microstructure and mechanical properties of Al-Zn-Mg-Cu-Zr based alloys. Rare Metals, 2009, 28(1): 102–106.

[10] Fang H C, Chao H, Chen K H. Effect of Zr, Er and Cr additions on microstructures and properties of Al-Zn-Mg-Cu alloys. Materials Science and Engineering: A, 2014, 610: 10–16.

[11] Gao Z, Li H, Lai Y, et al. Effects of minor Zr and Er on microstructure and mechanical properties of pure aluminum. Materials Science and Engineering: A, 2013, 580: 92–98.

[12] Li Q, Xia T, Lan Y, et al. Effects of rare earth Er addition on microstructure and mechanical properties of hypereutectic Al-20% Si alloy. Materials Science and Engineering: A, 2013, 588: 97–102.

[13] Martin A, Vilanova M, Gil E, et al. Influence of the Zr content on the processability of a high strength Al-Zn-Mg-Cu-Zr alloy by laser powder bed fusion. Materials Characterization, 2022, 183.

[14] Shi C, Chen X G. Effect of Zr addition on hot deformation behavior and microstructural evolution of AA7150 aluminum alloy. Materials Science and Engineering: A, 2014, 596: 183–193.

[15] Wu H, Wen S P, Huang H, et al. Effects of homogenization on precipitation of Al_3(Er, Zr) particles and recrystallization behavior in a new type Al-Zn-Mg-Er-Zr alloy. Materials Science and Engineering: A, 2017, 689: 313–322.

[16] Li B, Pan Q L, Chen C P, et al. Effect of aging time on precipitation behavior, mechanical and corrosion properties of a novel Al-Zn-Mg-Sc-Zr alloy. Transactions of Nonferrous Metals Society of China, 2016, 26(9): 2263–2275.

[17] Li B, Pan Q, Chen C, et al. Effects of solution treatment on microstructural and mechanical properties of Al-Zn-Mg alloy by microalloying with Sc and Zr. Journal of Alloys and Compounds, 2016, 664: 553–564.

[18] Wang G S, Zhao Z H, Zhang Y H, et al. Effects of solution treatment on microstructure and mechanical properties of Al-9.0Zn-2.8Mg-2.5Cu-0.12Zr-0.03Sc alloy. Transactions of Nonferrous Metals Society of China, 2013, 23(9): 2537–2542.

[19] Xu X, Jiang Z, Mao Q, et al. Effect of multi-stage solution and aging process on microstructure and properties of Al-10.7Zn-2.8Mg-1.2Cu-0.2Zr aluminum alloy extrusion materials. Materials Research Express, 2019, 6(6): 361–372.

[20] Tang H, Zhang Y, Sun Y, et al. Electron microscopy study of the impact of solution treatment on the corrosion behavior of an Al-Zn-Mg-Cu alloy. Corrosion Science, 2024, 226(1): 111665.

[21] Zhang Z, Li D, Li S, et al. Effect of direct aging treatment on microstructure, mechanical and corrosion properties of a Si-Zr-Er modified Al-Zn-Mg-Cu alloy prepared by selective laser melting technology. Materials Characterization, 2022, 194: 112459.

[22] Shi Y, Pan Q, Li M, et al. Influence of alloyed Sc and Zr, and heat treatment on microstructures and stress corrosion cracking of Al-Zn-Mg-Cu alloys. Materials Science and Engineering: A, 2015, 621: 173–181.

[23] Wang Y L, Jiang H C, Li Z M, et al. Two-stage double peaks ageing and its effect on stress corrosion cracking susceptibility of Al-Zn-Mg alloy. Journal of Materials Science & Technology, 2018, 34(7): 1250–1257.

[24] Gu K, Zeng X Q, Chen B, et al. Effect of double aging on mechanical properties and microstructure of EV31A alloy. Transactions of Nonferrous Metals Society of China, 2021, 31(9): 2606–2614.

[25] Liu Y, Jiang D M, Li W J. The effect of multistage ageing on microstructure and mechanical properties of 7050 alloy. Journal of Alloys and Compounds, 2016, 671: 408–418.

[26] Li H, Gao Z, Yin H, et al. Effects of Er and Zr additions on precipitation and recrystallization of pure aluminum. Scripta Materialia, 2013, 68(1): 59–62.

[27] Peng G, Chen K, Chen S, et al. Evolution of the second phase particles during the heating-up process of solution treatment of Al-Zn-Mg-Cu alloy. Materials Science and Engineering: A, 2015, 641: 237–241.

[28] Zhang Y H, Yang S C, Ji H Z. Microstructure evolution in cooling process of Al-Zn-Mg-Cu alloy and kinetics description. Transactions of Nonferrous Metals Society of China, 2012, 22(9): 2087–2091.

[29] Li N K, Lu X Y, Cui J Z. Effect of processing way and aging treatment on properties and microstructures of 7B04 aluminum alloy. Transactions of Nonferrous Metals Society of China, 2008, 18(3): 541–547.

[30] Zhang Z, Li D, Li S, et al. Effect of direct aging treatment on microstructure, mechanical and corrosion properties of a Si-Zr-Er modified Al-Zn-Mg-Cu alloy prepared by selective laser melting technology. Materials Characterization, 2022, 194: 112459.

[31] Sakai T, Otani Y, Sasaki S. Effect of heat treatment on hardness and microstructure of Mn-added Al-Cu-Mg-Zn-Si alloy fabricated by laser powder bed fusion. Journal of Japan Institute of Light Metals, 2022, 10: 172–185.

[32] Moshtaghi M, Mahdieh S, Tomohiko H. Effect of solution treatment temperature on grain boundary composition and environmental hydrogen embrittlement of an Al-Zn-Mg-Cu alloy. Vacuum, 2020, 184: 651–658.

[33] Chen Y L, Zhang C Y, Hou Y F, Xu Z Z. Effects of Mg and Sc additions on the microstructure and mechanical properties of Al-20Zn alloys. Materials Characterization, 2020, 159: 321–329.

[34] Trudonoshym O, Prach O, Randelzhofer P, et al. Heat treatment of the new high-strength high-ductility Al-Mg-Si-Mn alloys with Sc, Zr and Cr additions. Materialia, 2021, 15: 100981.